chemistry proceedings

MDPI

Proceeding Paper

Computational Investigations on Phycocyanobilin †

Matteo Gigli [1], Matteo Donati [1], Massimo Sgarzi [1] and Marco Bortoluzzi [1,2,*]

[1] Dipartimento di Scienze Molecolari e Nanosistemi, Università Ca' Foscari Venezia, Via Torino 155, 30170 Mestre, Veneto, Italy; matteo.gigli@unive.it (M.G.); 873903@stud.unive.it (M.D.); massimo.sgarzi@unive.it (M.S.)
[2] CIRCC, Consorzio Interuniversitario Reattività Chimica e Catalisi, Via Celso Ulpiani 27, 70126 Bari, Italy
* Correspondence: markos@unive.it; Tel.: +39-0412348561
† Presented at The 28th International Electronic Conference on Synthetic Organic Chemistry (ECSOC 2024), 15–30 November 2024; Available online: https://sciforum.net/event/ecsoc-28.

Abstract: Phycocyanobilin was computationally investigated by means of DFT calculations in combination with implicit solvation starting from X-ray data. Different conformations and degrees of protonation were considered, and the acidity constants were estimated. The computed data suggest a *syn-syn-syn* conformation for the molecule, with the two carboxylic groups deprotonated under physiological conditions and weak acidic behaviour of one of the pyrrolone heterocycles. The absorption transitions in the visible range were studied by means of TD-DFT calculations, focusing on the molecular orbitals involved. The frontier orbitals have a dominant role in the lowest energy absorption.

Keywords: phycocyanobilin; DFT calculations; acidity constant; electronic transitions

1. Introduction

Phycocyanobilin (PCB) is an antenna pigment found in cyanobacteria such as *Arthrospira Platensis* or *Synechococcus Elongatus*, and in some algae. From a structural point of view, PCB is a linear tetrapyrrole having two carboxyl groups and some hydrocarbon substituents, the terminal heterocycles actually being a pyrrolidinone and a pyrrolone, given the presence of a carbonyl function in *alpha* position with respect to the nitrogen atoms (Figure 1) [1–6]. PCB is a member of the bilines family, which are pigments such as phycoerythrobilin or biliverdin [7,8]. In nature, PCB is covalently bound via thioether bonding with cysteine, thus resulting in the prosthetic group of some proteins such as phycocyanin-C (C-PC), allophycocyanin or phycoerythrin. The interaction with sulfur involves the exocyclic double bond present in one of the terminal pyrrolones of the free PCB [9]. In general, phycobilins are bound to proteins having masses between 30 and 35 kDa. These proteins are then organized into higher structures called phycobilisomes located in the lamellar membranes of cyanobacteria and algae [10].

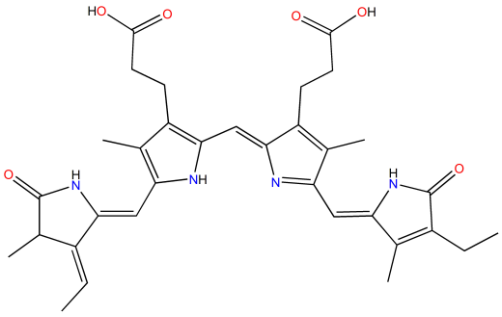

Figure 1. PCB sketched in neutral form and *anti-syn-anti* conformation.

Citation: Gigli, M.; Donati, M.; Sgarzi, M.; Bortoluzzi, M. Computational Investigations on Phycocyanobilin. *Chem. Proc.* **2024**, *6*, x. https://doi.org/10.3390/xxxxx

Academic Editor(s): Name

Published: 15 November 2024

The main biological role of pigments such as PCB is to assist the photosynthetic process by acting as antennae, i.e., collecting radiant energy from the sun and transferring it to the photosynthetic reaction centers. The commonly accepted mechanism is the Förster resonance energy transfer [11]. Such a role is evidenced by the lowest energy absorption band in the visible range of PCB-containing species, which is located in the red region of the spectrum and exhibits a pH-dependent nature. The luminescence of PCB in C-PC corresponds to an emission band centred at about 650 nm, with scarce Stokes shift with respect to the main absorption band [12,13]. Unlike porphyrins and related cyclic systems, the open tetrapyrrole structure of PCB has not been found to be associated with metal centers in biological derivatives subjected to structural studies. Investigations carried out on PCB obtained by a solvolitic approach showed a progressive quenching of luminescence by addition of Hg(II) [14].

Given the intriguing features of PCB as bio-based choromophore of commercial interest [15–17], the electronic structure of the molecule and selected related spectroscopic properties were investigated using computational methods based on the DFT and TDDFT theories and here summarized.

2. Computational Methods

The optimization of the hydrogen atoms added to the $\{C_{33}N_4O_6\}$ skeleton derived from experimental data was carried out with the Merck Molecular Force Field (MMFF) [18], keeping the other atoms frozen. The software used was Spartan '16 version 2.0.3 [19]. The geometry optimizations were initially performed using the PBEh-3c method, a reparametrized version of the PBE0 hybrid functional (42% HF exchange) [20] that uses a split-valence double-zeta basis set (def2-mSVP) [21,22] and adds three corrections considering dispersion, basis set superposition and other basis set incompleteness effects [23–25]. Further calculations were carried out with the r^{2}SCAN-3c method [26], based on the meta-GGA r^{2}SCAN functional [27] combined with a tailor-made triple-ζ Gaussian atomic orbital basis set. The method also includes refitted D4 and geometrical counter-poise corrections for London dispersion and basis set superposition error [23,28]. A third DFT method used was based on the TPSSh hybrid meta-GGA DFT functional [29] in combination with Ahlrichs' def2-TZVP basis set [21]. The C-PCM implicit solvation model was added, considering water as a continuous medium [30]. IR simulations were carried out using the harmonic approximation, from which zero-point vibrational energies and thermal corrections (T = 298.15 K) were obtained. The electronic transitions were simulated by means of TDDFT calculations, considering 12 singlet and 12 triplet roots and including the spin-orbit correction [31]. Calculations were carried out using ORCA version 5.0.3 [32,33] and the output files were analysed with Multiwfn version 3.8 [34].

3. Results and Discussion

In order to construct the molecular models of PCB, the deposited structure of C-PC in *Synechococcus Elongatus* (1.45 Å resolution) was considered as starting point [35]. The PCB choromophore was isolated from the surrounding protein chains and the hydrogen atoms were added coherently with the accepted Lewis structure. The positions of the hydrogen atoms were initially optimized by means of the MMFF method, keeping frozen the other atoms. The relative orientations of the four heterocycles in the starting structure determine an *anti-syn-anti* conformation (Figure 1).

All the DFT calculations were carried out in combination with the C-PCM implicit solvation model, considering water as continuous medium. The molecule was initially optimized in its neutral form, indicated as $[PCB_{ASA}]^0$, by means of the PBEh-3c, r^{2}SCAN-3c and TPSSh/def2-TZVP methods. The geometry optimizations afforded comparable stationary points and maintained the initial *anti-syn-anti* conformation. Given the presence of four acidic protons, all the possible $[PCB_{ASA}]^{1-}$ monoanions derived from the formal deprotonation of $[PCB_{ASA}]^0$ were optimized with the PBEh-3c method. The structures are

sketched in Figure 2 with their relative Gibbs energy values. The most stable $[PCB_{ASA}]^{1-}$ isomer was optimized again using the TPSSh/def2-TZVP approach and its Gibbs energy value, together with that of $[PCB_{ASA}]^{0}$, was used for the estimation of the pK_{a1} value, calculated on the basis of a formal acid-base reaction between PCB and a chemically related species with known pK_a. Given the presence of the carboxylic groups in PCB, the acetic acid (HOAc)/acetate (OAc^-) couple was considered as a proper reference ($pK_a^{HOAc} = 4.756$). The general reaction is thus $[PCB_{ASA}]^{n-} + OAc^- \rightarrow [PCB_{ASA}]^{(n+1)-} + HOAc$. The acidity constants of PCB were obtained according to equation 1, where ΔG represents the calculated Gibbs energy variation for the reaction, R is the gas constant and T is the temperature (298 K). Starting from the most stable $[PCB_{ASA}]^{1-}$ isomer, the $[PCB_{ASA}]^{2-}$ dianions were then optimized at the PBEh-3c level (Figure 2) and the isomer having the lowest Gibbs energy was used for the estimation of the pK_{a2} value after further optimization with the TPSSh/def2-TZVP method. The same procedure was repeated for the third deprotonation, with the determination of the most stable $[PCB_{ASA}]^{3-}$ isomer (Figure 2). Table 1 collects the calculated pK_a values. According to the pK_a values, the two carboxyl groups of the *anti-syn-anti* conformer of PCB should be deprotonated at physiological pH.

$$pK_a^{PCB} = 4.756 + \Delta G/(2.303RT) \quad (1)$$

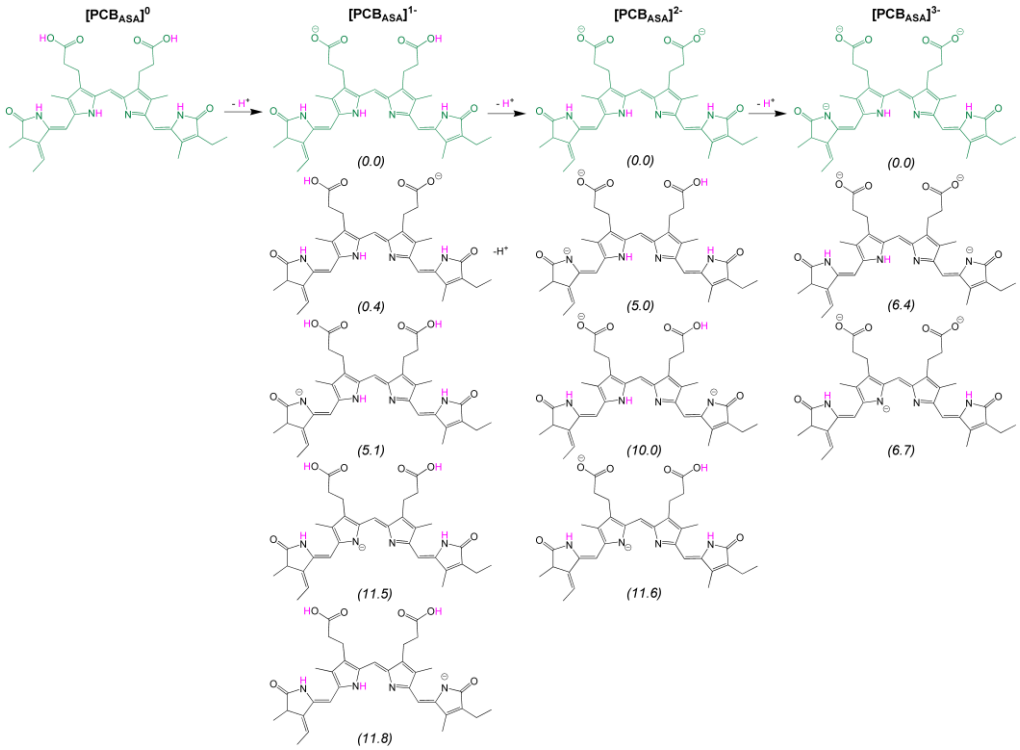

Figure 2. Isomers of $[PCB_{ASA}]^{n-}$ (n = 0, 1, 2, 3) with relative Gibbs energy values (kcal mol^{-1}, C-PCM/PBEh-3c calculations) in parenthesis. The most stable isomers are coloured in green.

Table 1. Computed pK_a values for PCB_{ASA} and PCB_{SSS}. C-PCM/TPSSh/def2-TZVP calculations.

	PCB_{ASA}	**PCB_{SSS}**
pK_{a1}	3.1	3.3
pK_{a2}	4.1	4.3
pK_{a3}	10.5	6.9

The value of root mean square deviation (RMSD) between the TPSSh/def2-TZVP optimized $\{C_{33}N_4O_6\}$ skeletons of $[PCB_{ASA}]^{2-}$ and the corresponding X-ray data is 1.00 Å. r^2SCAN-3c calculations afforded a strictly comparable stationary point, with a RMSD of

0.83 Å with respect to the experimental structure. The differences occurring between the computed structures and the starting geometry used are attributable to the removal of the apoprotein before the calculations and to the flexibility of some of the substituents on the heterocycles.

Relaxed surface scan calculations indicated that the energy barriers for the rotation of the external methenylpyrrolone units with respect of the central methenyldipyrrolic fragment are around 5 kcal mol^{-1}, marking other conformations of the free molecule accessible at room temperature. The plots of the relative energy values vs. the dihedral angles are shown in Figure 3. Moreover, the *syn-syn-syn* conformers of PCB, generally indicated with $[PCB_{SSS}]^{n-}$ (n = 0, 1, 2, 3) resulted thermodynamically more stable than the corresponding $[PCB_{ASA}]^{n-}$ conformers, as already stated in previous studies [36]. The Gibbs energy differences (ΔG) between $[PCB_{SSS}]^{n-}$ and $[PCB_{ASA}]^{n-}$ range between 6.4 and 11.6 kcal mol^{-1}, depending upon the charge of the species. The ΔG values are collected in Table 2.

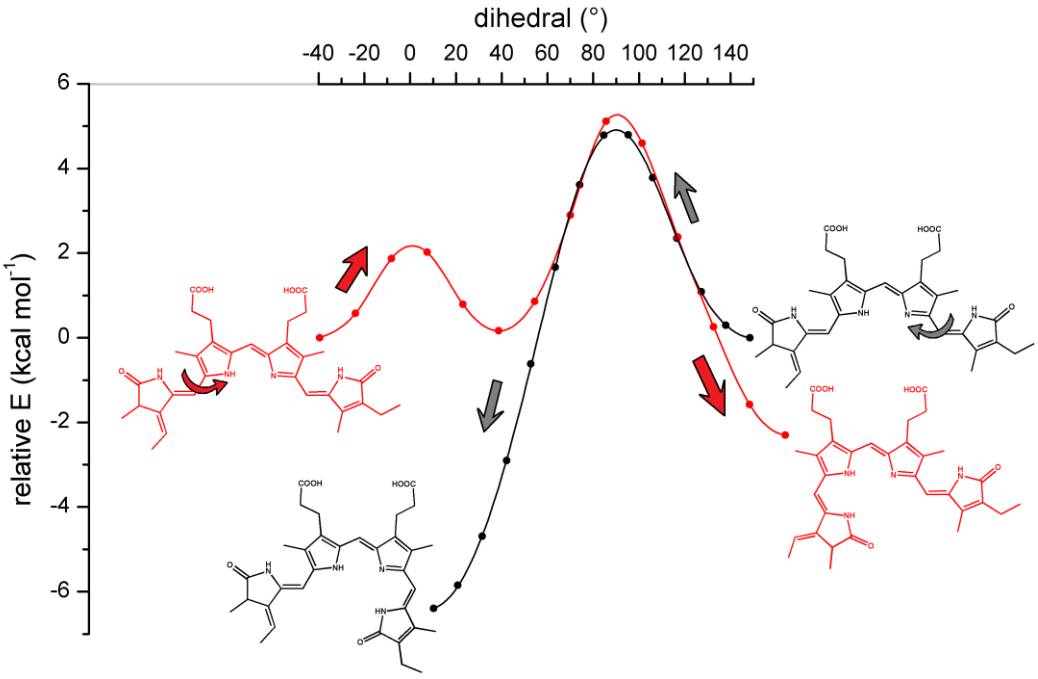

Figure 3. Relative energies (kcal mol^{-1}) vs. the dihedral angles between the external pyrrolones and the central dipyrrole fragment. C-PCM/r²SCAN-3c calculations.

Table 2. Gibbs energy differences (kcal mol^{-1}) between the $[PCB_{SSS}]^{n-}$ and $[PCB_{ASA}]^{n-}$ conformers (n, 0, 1,2, 3). C-PCM/TPSSh/def2-TZVP calculations.

n	ΔG
0	−8.9
1	−6.4
2	−6.7
3	−11.6

Since the computational outcomes suggest the *syn-syn-syn* conformation as the most stable for the free molecule in solution, the estimation of the acidity constants was repeated. The pK_a values are reported in Table 1. The change of conformation strongly lowers the pK_{a3} value, calculated around 6.9 for the *syn-syn-syn* conformer. Free PCB should be therefore present under physiological conditions in equilibrium between its doubly and triply deprotonated forms.

The C-PCM/TPSSh/def2-TZVP optimized structures of $[PCB_{SSS}]^{2-}$ and $[PCB_{SSS}]^{3-}$ are shown in Figure 4. As for all the DFT-optimized structures here considered, the stationary

points were characterized as local minima by means of IR simulations. On considering selected computed spectral features, the simulated bands having the highest wavenumbers, excluding the C-H and N-H stretchings, are associated to the pyrrolone carbonyl stretchings both for $[PCB_{SSS}]^{2-}$ and $[PCB_{SSS}]^{3-}$. The unscaled computed wavenumbers depend upon the charge of the molecule, being 1725 and 1662 cm^{-1} for $[PCB_{SSS}]^{2-}$ and 1650 and 1649 cm^{-1} for $[PCB_{SSS}]^{3-}$.

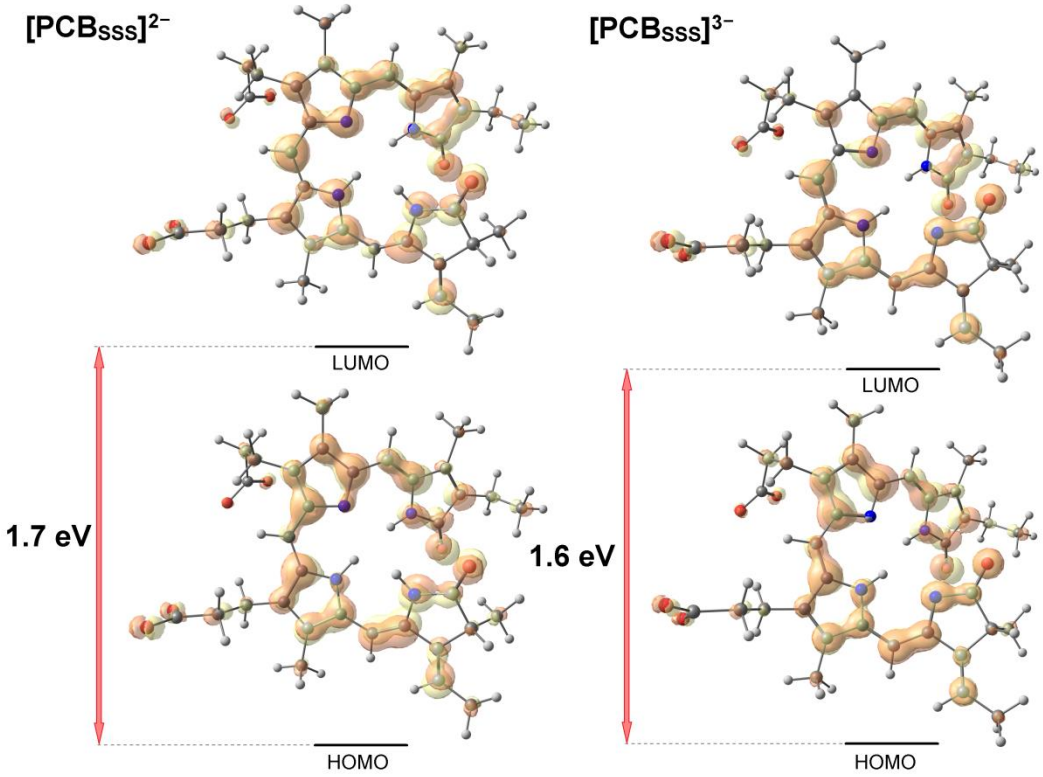

Figure 4. DFT-optimized structures of $[PCB_{SSS}]^{2-}$ and $[PCB_{SSS}]^{3-}$ with plots of the frontier orbitals (yellow/orange, surface isovalue = 0.03 a.u.) and HOMO-LUMO gaps. Colour map: O, red; N, blue; C, grey; H, white.

TDDFT calculations at C-PCM/TPSSh/def2-TZVP level predicted the lowest energy $S_1 \leftarrow S_0$ absorptions at 610 nm (oscillator strength = 0.71) for $[PCB_{SSS}]^{2-}$ and at 647 nm (oscillator strength = 0.66) for $[PCB_{SSS}]^{3-}$, in line with the experimental interval [12,13]. In both cases the transition has 100% LUMO←HOMO character. The red shift of the absorption moving from the dianion to the trianion agrees with the calculated 0.1 eV lowering of the HOMO-LUMO gap. The frontier molecular orbitals are shown in Figure 4. The transitions involve the π-delocalized electronic structure on the conjugated tetrapyrrolic structure, as clearly observable also from the plots of the hole and electron distributions in Figure 5 [37]. The PCB molecule can be considered aromatic, as indicated by the Shannon aromaticity index (SA) computed from the electron density values at the C-C, C-N and C-O bond critical points [38]. The SA values are equal to 5×10^{-3} both for $[PCB_{SSS}]^{2-}$ and $[PCB_{SSS}]^{3-}$. The alterations of the electronic structures caused by the $S_1 \leftarrow S_0$ transitions are better highlighted by plotting the differences between the hole and the electron distributions, an approach known as Charge Density Difference [37] (Figure 5). For instance, the lowest energy absorption makes the methine group bonded to the terminal pyrrolidinone electron poorer, while the opposite situation occurs for the other two bridging {CH} fragments.

It is worth noting that the lowest energy absorptions are predicted with a blue-shift around 45 nm for the related $[PCB_{ASA}]^{n-}$ conformers, highlighting that the conformation assumed by the tetrapyrrolic unit influences the spectral features of PCB-containing species [39]. On considering other degrees of protonation, the lowest energy $S_1 \leftarrow S_0$ absorption

is calculated at 609 nm for both $[PCB_{SSS}]^{0}$ and $[PCB_{SSS}]^{1-}$. The TDDFT calculations here reported suggest that the absorption features of PCB become pH-dependent when the acid-base equilibrium involves one of the N-heterocycles, while the protonation of the carboxylic groups negligibly influences the absorption maximum.

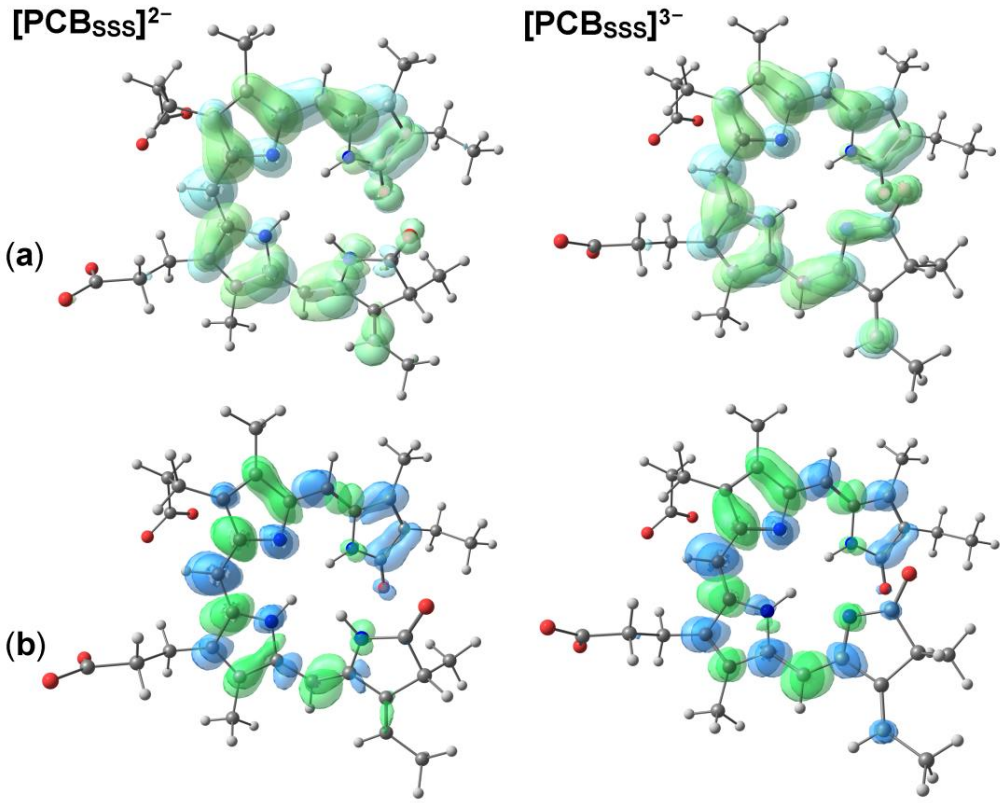

Figure 5. (**a**) Superpositions of the hole (light green) and electron (light blue) distributions related to the $S_1 \leftarrow S_0$ transitions in $[PCB_{SSS}]^{2-}$ and $[PCB_{SSS}]^{3-}$. (**b**) Charge Density Difference plots, with the regions with excess of hole and excess of electron distributions green and blue coloured, respectively. Colour map: O, red; N, blue; C, grey; H, white. Surfaces isovalue = 0.001 a.u.

The addition of SOC to the calculations caused negligible effects to the predicted transitions, a result expected given the lack of heavy atoms in the structure. The lowest energy forbidden $T \leftarrow S_0$ absorption was predicted for both $[PCB_{SSS}]^{2-}$ and $[PCB_{SSS}]^{3-}$ in the NIR range, at 1131 nm for the dianion and 1200 nm for the trianion. The luminescence quenching observed by adding a heavy metal ion such as Hg^{2+} [14] can be explained on admitting an increased rate of intersystem crossing towards triplet excited states, followed by non-radiative decay given the quite low energy gap. To better investigate this point, the triplet state geometries of $[PCB_{SSS}]^{2-}$ and $[PCB_{SSS}]^{3-}$ were optimized. The RMSD values with respect to the singlet ground state geometries are low, with values equal to 0.193 Å for $[PCB_{SSS}]^{2-}$ and 0.075 Å for $[PCB_{SSS}]^{3-}$. The hypothetic $T \rightarrow S_0$ phosphorescent decays are predicted to have low energy, being the computed wavelengths equal to 1520 nm for the dianion and 1495 nm for the trianion. As for the $S_1 \leftarrow S_0$ absorptions, these transitions involve only the two frontier orbitals.

4. Conclusions

The computational outcomes here provided support the comprehension of the acid-base behaviour of PCB, which influences the absorption features of the molecule. Another factor that affects the absorption maximum in the red range is the conformation assumed by the tetrapyrrolic fragment, that resulted noticeably different on comparing the free molecule and PCB-containing proteins. All these parameters should be considered when

PCB is embedded in a matrix and applied as bio-based pigment. Moreover, the use of PCB as luminescent sensor for heavy metal ions can be rationalized on considering the low energy values computed for the triplet excited states, which favour non-radiative decay routes.

Author Contributions: Conceptualization, M.G., M.S. and M.B.; methodology, M.B. and M.D.; validation, M.G., M.S. and M.B.; formal analysis, M.D. and M.B.; investigation, M.D. and M.B.; resources, M.G. and M.B.; data curation, M.D. and M.B.; writing—original draft preparation, M.B.; writing—review and editing, M.G. and M.S.; visualization, M.D. and M.B.; supervision, M.S., M.G. and M.B.; project administration, M.B.; funding acquisition, M.G. All authors have read and agreed to the published version of the manuscript.

Funding: This research was funded by the European Union Next-GenerationEU—National Recovery and Resilience Plan (NRRP)—MISSION 4 COMPONENT 2, INVESTIMENT 1.1 Fondo per il Programma Nazionale di Ricerca e Progetti di Rilevante Interesse Nazionale (PRIN)—CUP N. H53D23007900001, project: "Thorough Upcycling of Rice waste biomass into BiOactive PACKaging via chemoenzymatic processes (TURBOPACK)". This work is part of the "Network 4 Energy Sustainable Transition-NEST" project (MIUR project code PE000021, Concession Degree No. 1561 of 11 October 2022), in the framework of the NextGenerationEu PNRR plan (CUP C93C22005230007).

Institutional Review Board Statement:

Informed Consent Statement:

Data Availability Statement: Dataset available on request from the authors.

Acknowledgments: CINECA (Bologna) is acknowledged for the availability of high-performance computing resources (class C project INLIGHT).

Conflicts of Interest: The authors declare no conflict of interest. The funders had no role in the design of the study; in the collection, analyses, or interpretation of data; in the writing of the manuscript, or in the decision to publish the results.

References

1. Crespi, H.L.; Boucher, L.J.; Norman, G.D.; Katz, J.J.; Dougherty, R.C. Structure of phycocyanobilin. *J. Am. Chem. Soc.* **1967**, *89*, 3642–3643. https://doi.org/10.1021/ja00990a054.
2. Cole, W.J.; Chapman, D.J.; Siegelman, H.W. Structure of phycocyanobilin. *J. Am. Chem. Soc.* **1967**, *89*, 3643–3645. https://doi.org/10.1021/ja00990a055.
3. Rüdiger, W.; Carra, P.; Heocha, C.Ó. Structure of Phycoerythrobilin and Phycocyanobilin. *Nature* **1967**, *215*, 1477–1478. https://doi.org/10.1038/2151477a0.
4. Cole, W.J.; Chapman, D.J.; Siegelman, H.W. Structure and properties of phycocyanobilin and related bilatrienes. *Biochemistry* **1968**, *7*, 2929–2935. https://doi.org/10.1021/bi00848a033.
5. Schram, B.L.; Kroes, H.H. Structure of Phycocyanobilin. *Eur. J. Biochem*. **1971**, *19*, 581–594. https://doi.org/10.1111/j.1432-1033.1971.tb01352.x.
6. Fu, E.; Friedman, L.; Siegelman, H.W. Mass-spectral identification and purification of phycoerythrobilin and phycocyanobilin. *Biochem. J.* **1979**, *176*, 1–6. https://doi.org/10.1042/bj1790001.
7. Brown, S.B.; Houghton, J.D.; Vernon, D.I. New trends in photobiology. Biosynthesis of phycobilins. Formation of the chromophore of phytochrome, phycocyanin and phycoerythrin. *J. Photochem. Photobiol. B* **1990**, *5*, 3–23. https://doi.org/10.1016/1011-1344(90)85002-E.
8. Rockwell, N.C.; Martin, S.S.; Lagarias, J.C. Elucidating the origins of phycocyanobilin biosynthesis and phycobiliproteins. *Proc. Natl. Acad. Sci. USA* **2023**, *120*, e2300770120. https://doi.org/10.1073/pnas.2300770120.
9. Bishop, J.E.; Lagarias, J.C.; Nagy, J.O.; Schoenleber, R.W.; Rapoport, H. Phycobiliprotein-bilin linkage diversity. I. Structural studies on A- and D-ring-linked phycocyanobilins. *J. Biol. Chem.* **1986**, *261*, 6790–6796. https://doi.org/10.1016/S0021-9258(19)62685-2.
10. Minato, T.; Teramoto, T.; Adachi, N.; Hung, N.K.; Yamada, K.; Kawasaki, M.; Akutsu, M.; Moriya, T.; Senda, T.; Ogo, S.; et al. Non-conventional octameric structure of C-phycocyanin. *Commun. Biol.* **2021**, *4*, 1238. https://doi.org/10.1038/s42003-021-02767-x.
11. Croce, R.; van Amerongen, H. Natural strategies for photosynthetic light harvesting. *Nat. Chem. Biol.* **2014**, *10*, 492–501. https://doi.org/10.1038/nchembio.1555.
12. hEocha, C.Ó. Spectral Properties of the Phycobilins. I. Phycocyanobilin. *Biochemistry* **1963**, *2*, 375–382. https://doi.org/10.1021/bi00902a034.

13. Bischoff, M.; Hermann, G.; Rentsch, S.; Strehlow, D.; Winter, S.; Chosrowjan, H. Excited-State Processes in Phycocyanobilin Studied by Femtosecond Spectroscopy. *J. Phys. Chem. B* **2000**, *104*, 1810–1816. https://doi.org/10.1021/jp992083f.
14. Suresh, M.; Mishra, S.K.; Mishra, S.; Das, A. The detection of Hg^{2+} by cyanobacteria in aqueous media. *Chem. Commun.* **2009**, 2496–2498. https://doi.org/10.1039/B821687H.
15. Roda-Serrat, M.C.; Christensen, K.V.; El-Houri, R.B.; Fretté, X.; Christensen, L.P. Fast cleavage of phycocyanobilin from phycocyanin for use in food colouring. *Food Chem.* **2018**, *240*, 655–661. https://doi.org/10.1016/j.foodchem.2017.07.149.
16. Alhefeiti, M.; Chandra, F.; Gupta, R.K.; Saleh, N. Dyeing Non-Recyclable Polyethylene Plastic with Photoacid Phycocyanobilin from Spirulina Algae: Ultrafast Photoluminescence Studies. *Polymers* **2022**, *14*, 4811. https://doi.org/10.3390/polym14224811.
17. Tang, K.; Beyer, H.M.; Zurbriggen, M.D.; Gärtner, W. The Red Edge: Bilin-Binding Photoreceptors as Optogenetic Tools and Fluorescence Reporters. *Chem. Rev.* **2021**, *121*, 14906–14956. https://doi.org/10.1021/acs.chemrev.1c00194.
18. Halgren, T.A. Merck molecular force field. I. Basis, form, scope, parameterization, and performance of MMFF94. *J. Comput. Chem.* **1996**, *17*, 490–519. https://doi.org/10.1002/(SICI)1096-987X(199604)17:5/6<490::AID-JCC1>3.0.CO;2-P.
19. *Spartan '16*; Build 2.0.3; Wavefunction Inc.: Irvine, CA, USA, 2016.
20. Grimme, S.; Brandenburg, J.G.; Bannwarth, C.; Hansen, A.A. Consistent structures and interactions by density functional theory with small atomic orbital basis sets. *J. Chem. Phys.* **2015**, *143*, 054107. https://doi.org/10.1063/1.4927476.
21. Weigend, F.; Ahlrichs, R. Balanced basis sets of split valence, triple zeta valence and quadruple zeta valence quality for H to Rn: Design and assessment of accuracy. *Phys. Chem. Chem. Phys.* **2005**, *7*, 3297–3305. https://doi.org/10.1039/B508541A.
22. Weigend, F. Accurate Coulomb-fitting basis sets for H to Rn. *Phys. Chem. Chem. Phys.* **2006**, *8*, 1057–1065. https://doi.org/10.1039/B515623H.
23. Kruse, H.; Grimme, S. A geometrical correction for the inter- and intra-molecular basis set superposition error in Hartree-Fock and density functional theory calculations for large systems. *J. Chem. Phys.* **2012**, *136*, 154101. https://doi.org/10.1063/1.3700154.
24. Grimme, S.; Ehrlich, S.; Goerigk, L. Effect of the damping function in dispersion corrected density functional theory. *J. Comput. Chem.* **2011**, *32*, 1456–1465. https://doi.org/10.1002/jcc.21759.
25. Grimme, S.; Antony, J.; Ehrlich, S.; Krieg, H. A consistent and accurate ab initio parametrization of density functional dispersion correction (DFT-D) for the 94 elements H-Pu. *J. Chem. Phys.* **2010**, *132*, 154104. https://doi.org/10.1063/1.3382344.
26. Grimme, S.; Hansen, A.; Ehlert, S.; Mewes, J.-M. r^2SCAN-3c: A "Swiss army knife" composite electronic-structure method. *J. Chem. Phys.* **2021**, *154*, 064103. https://doi.org/10.1063/5.0040021.
27. Furness, J.W.; Kaplan, A.D.; Ning, J.; Perdew, J.P.; Sun, J. Accurate and Numerically Efficient r^2SCAN Meta-Generalized Gradient Approximation. *J. Phys. Chem. Lett.* **2020**, *11*, 8208–8215. https://doi.org/10.1021/acs.jpclett.0c02405.
28. Caldeweyher, E.; Ehlert, S.; Hansen, A.; Neugebauer, H.; Spicher, S.; Bannwarth, C.; Grimme, S.A. Generally applicable atomic-charge dependent London dispersion correction. *J. Chem. Phys.* **2019**, *150*, 154122. https://doi.org/10.1063/1.5090222.
29. Staroverov, V.N.; Scuseria, E.; Tao, J.; Perdew, J.P.Comparative assessment of a new nonempirical density functional: Molecules and hydrogen-bonded complexes. *J. Chem. Phys.* **2003**, *119*, 12129–12137. https://doi.org/10.1063/1.1626543.
30. Cossi, M.; Rega, N.; Scalmani, G.; Barone, V. Energies, structures, and electronic properties of molecules in solution with the C-PCM solvation model. *J. Comput. Chem.* **2003**, *24*, 669–681. https://doi.org/10.1002/jcc.10189.
31. de Souza, B.; Farias, G.; Neese, F.; Izsák, R. Predicting Phosphorescence Rates of Light Organic Molecules Using Time-Dependent Density Functional Theory and the Path Integral Approach to Dynamics. *J. Chem. Theory Comput*. **2019**, *15*, 1896–1904. https://doi.org/10.1021/acs.jctc.8b00841.
32. Neese, F. The ORCA program system, *WIREs Comput. Mol. Sci.* **2012**, *2*, 73–78. https://doi.org/10.1002/wcms.81.
33. Neese, F. Software update: The ORCA program system–Version 5.0. *WIREs Comput. Mol. Sci.* **2022**, *12*, e1606. https://doi.org/10.1002/wcms.1606.
34. Lu, T.; Chen, F. Multiwfn: A multifunctional wavefunction analyser. *J. Comput. Chem.* **2012**, *33*, 580–592. https://doi.org/10.1002/jcc.22885.
35. Nield, J.; Rizkallah, P.J.; Barber, J.; Chayen, N.E. The 1.45 Å three-dimensional structure of C-phycocyanin from the thermophilic cyanobacterium *Synechococcus elongatus*. *J. Struct. Biol.* **2003**, *141*, 149–155. https://doi.org/10.1016/S1047-8477(02)00609-3.
36. Göller, A.H.; Strehlow, D.; Hermann, G. Conformational Flexibility of Phycocyanobilin: An AM1 Semiempirical Study. *ChemPhysChem* **2001**, *2*, 665–671. https://doi.org/10.1002/1439-7641(20011119)2:11<665::AID-CPHC665>3.0.CO;2-O.
37. Liu, Z.; Lu, T.; Chen, Q. An sp-hybridized all-carboatomic ring, cyclo [18]carbon: Electronic structure, electronic spectrum, and optical nonlinearity. *Carbon* **2020**, *165*, 461–467. https://doi.org/10.1016/j.carbon.2020.05.023.
38. Noorizadeh, S.; Shakerzadeh, E. Shannon entropy as a new measure of aromaticity, Shannon aromaticity. *Phys. Chem. Chem. Phys.* **2010**, *12*, 4742–4749. https://doi.org/10.1039/B916509F.
39. Glazer, A.N.; Fang, S.; Brown, D.M. Spectroscopic Properties of C-Phycocyanin and of Its α and β Subunits. *J. Biol. Chem.* **1973**, *248*, 5679–5685. https://doi.org/10.1016/S0021-9258(19)43559-X.